High-temperature behavior of impurities and dimensionality of the charge transport in unintentionally and tin-doped indium selenide

J. Martinez-Pastor and A. Segura
Departament de Física Aplicada, Facultat de Física, Universitat de València, 46100 Burjassot, València, Spain

A. Chevy
Laboratoire de Physique des Milieux très Condensés, 4 Place Jussieu, Tour 13, 4eme étage, 75005 Paris, France

(Received 10 March 1993; accepted for publication 26 May 1993)

A systematic study of the electron transport and shallow impurity distribution in indium selenide above room temperature or after an annealing process is reported by means of far-infrared-absorption and Hall-effect measurements. Evidences are found for the existence of a large concentration of deep levels (10^{12}–10^{13} cm^{-2}), related to impurities adsorbed to stacking faults in this material. Above room temperature impurities can migrate from those defect zones and then become shallow in the bulk. The subsequent large increase of 3D electrons can change the dimensionality of the electron transport, which in most cases was 2D. The temperature dependence of the resistivity parallel to the c axis can be explained by the observed increase of the 3D electron concentration, whose motion across the layers is limited by stacking-fault-related potential barriers. The observed macroscopic resistivity is thus determined by tunneling through those barriers.

I. INTRODUCTION

Indium selenide (InSe) is a III-VI layered semiconductor, which is usually grown by the Bridgman method. Unintentionally doped crystals exhibit n character due to a native shallow donor level, which has been attributed to interstitial indium atoms homogeneously distributed through the crystal.[1–3]

One of the main features of electron transport in InSe is the presence of naturally occurring 2D electron layers related to stacking faults with an areal concentration of the order of 10^{11} cm^{-2}. These 2D electron layers were first attributed to the existence of 2D electric subbands in electron accumulation layers, created by planar aggregates of donor impurities bound to stacking faults.[4] Recently a microscopic model has been proposed which could explain the origin of the 2D electrons and their influence on the effective charge transport.[5] This model assumes the existence of thin layers ($\approx$100 Å) of the ϵ polytype of InSe ($P6m2$ spatial group) alternating with the predominant γ polytype ($R3m$ spatial group), which are separated by stacking faults. The potential barriers originated in the stacking faults would provide a natural size quantization zone on the thin ϵ layer, and then all electronic levels would be raised, in such a way that the shallow donor level is higher than the energy of the conduction band of the γ polytype. Consequently, the electrons of these donors would be transferred outside the thin ϵ layers and localized in 2D subbands by the electric field of those ionized impurities and the potential barrier associated to the stacking faults. The ϵ layers are then depleted of electrons, which explains the high resistivity measured along the c axis.

In this work we apply that model to give an account of the temperature dependence of the Hall coefficient and resistivity anisotropy above room temperature, as well as low-temperature results on annealed samples. The experimental procedures in this work are outlined in Sec. II. The results from electrical and far-infrared-absorption measurements are described in Sec. III. Section IV contains a discussion of these results on the basis of the microscopic model proposed in Ref. 5.

II. EXPERIMENT

InSe crystals have been grown by the Bridgman method from a nonstoichiometric polycrystalline melt $In_{1.05}Se_{0.95}$. Tin is introduced in the polycrystalline melt as a compound, SnSe.[6] The percentages of tin were 0.01%, 0.03%, 0.1%, 1%, and 3%. Only a small portion of the doping agent remains in the crystal, the rest being segregated to the end of the ingot.[7] That is, actual concentration of these substitutional impurities in our material is several orders of magnitude lower than that incorporated in the initial melt, as shown by far-infrared measurements.[3] We only maintain the Sn percentages for referring to the different samples.

The samples were cleaved along the layers from the ingots with a razor blade and cut into parallelepipeds 10–20 μm thick and about 3×5 mm^2 in size, for resistivity and Hall-effect (HE) measurements perpendicular to the c axis, and 200–500 μm thick for resistivity along the c axis. Electric contacts were made by vacuum evaporation of indium. Contacts for HE were prepared in the classic configuration. For resistivity measurements along the c axis three contacts were deposited on each face: Current flows through the largest contacts that occupy nearly 80% of each face. The two smaller contacts on each face are used to measure the ohmic voltage and to test the homogeneity of the sample.

 0021-8979/93/74(5)/3231/7/$6.00

The electrical measurements in the high-temperature region (300–700 K) were performed in vacuum ($<10^{-4}$ Torr) to avoid surface oxidation and the magnetic field was 0.3 T. The HE measurements in annealed samples, from 30 to 300 K, were made in a closed-cycle cryogenic system and with a magnetic field of 0.6 T. The annealing was also carried out in vacuum ($<10^{-4}$ Torr) for 15–30 min at 300 °C.

Far-infrared transmittance was performed in a Brüker Fourier transform spectrometer. An Oxford cryostat, temperature controller, and helium pumping system were used to achieve low temperatures. The nonannealed samples were thicker than 500 μm and about the annealed ones 100 μm thick, given their larger absorption coefficient.

III. RESULTS

A. Electrical characterization

When one studies the temperature dependence of electron concentration in InSe with low Sn content one finds that shallow donors become ionized between 20 and 100 K.[8] Above this temperature and below 300 K the electron concentration is fairly constant, as if the exhaustation regime was attained. Figure 1(a) shows the behavior of such samples above room temperature (RT). Above 380 K the electron concentration exhibits again an activated behavior, with activation energies of about 200 meV. At about 600 K the Hall concentration saturates again and, what is more remarkable, after returning to room temperature [Fig. 1(a)], it remains of order of 2×10^{16} cm^{-3}. The temperature dependence of the Hall mobility μ_H above RT also exhibits an unexpected behavior. Figure 1(b) shows the variation of the Hall mobility in a cycle of temperature

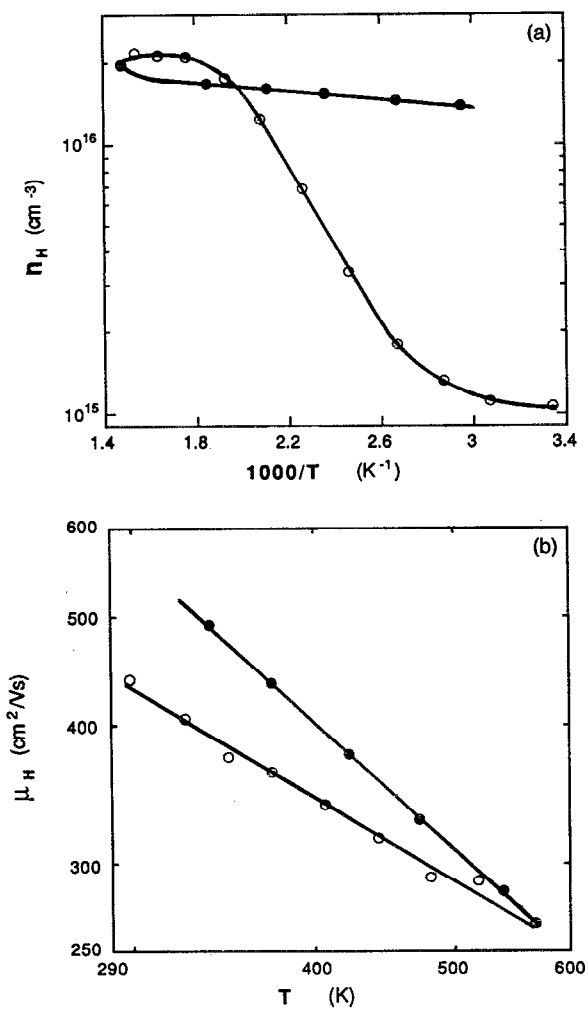

FIG. 1. Hall (a) concentration and (b) mobility for a 0.01% Sn-doped sample in a closed-cycle temperature variation above RT. The open symbol refers to measurements with increasing temperature, the closed symbol to those made from the highest temperature down to 300 K. Solid lines are guides for the eyes.

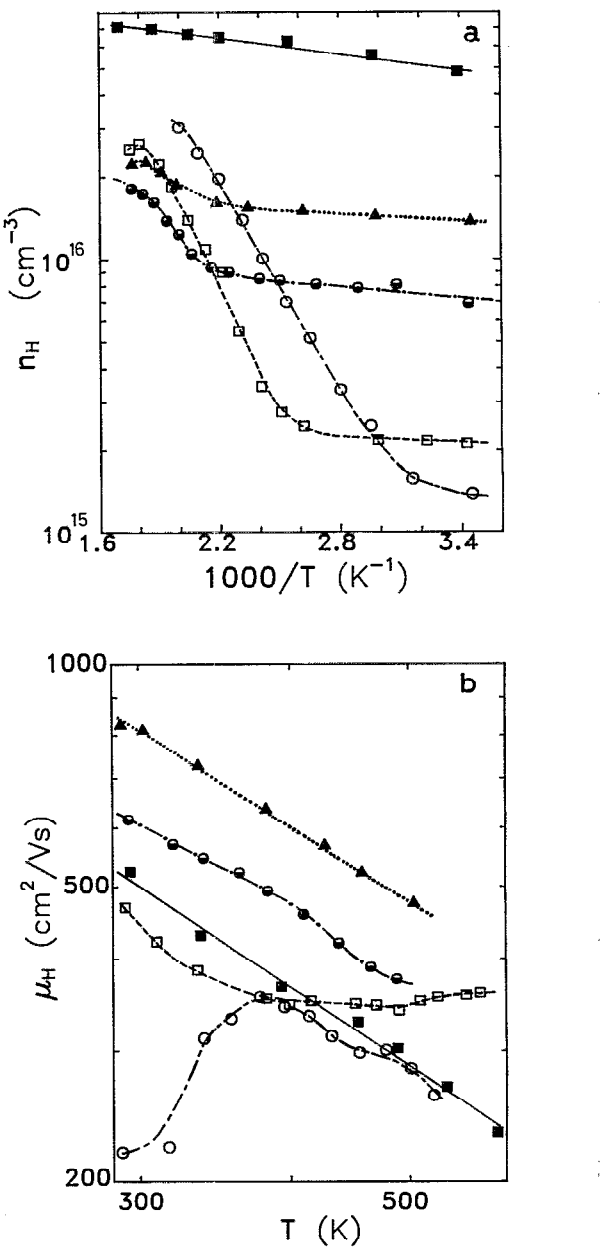

FIG. 2. Temperature dependence above RT of the Hall (a) concentration and (b) mobility for representative samples of the different Sn-doped ingots: (○) 0.01%, (□) 0.03%, (◒) 0.1%, (▲) 1%, and (■) 3%. Lines are guides for the eyes.

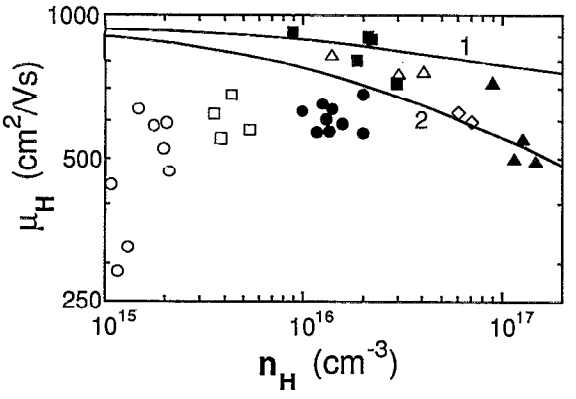

FIG. 3. Hall mobility as a function of the Hall concentration at RT for samples of the different Sn-doped ingots: (○) 0.01% and 0.03%, (□) 0.1%, (△) 1%, (◇) 3%, (▲) 10%, (■) 0.01% after annealing at 300 °C for 30 min, and (●) samples from 0.01% and 0.03% ingots after heating at 200–300 °C and returning to RT. Solid lines correspond to the calculated variation of the Hall mobility with impurity concentration without compensation (curve 1) and assuming a compensation degree of 0.6 (curve 2) (see Ref. 5).

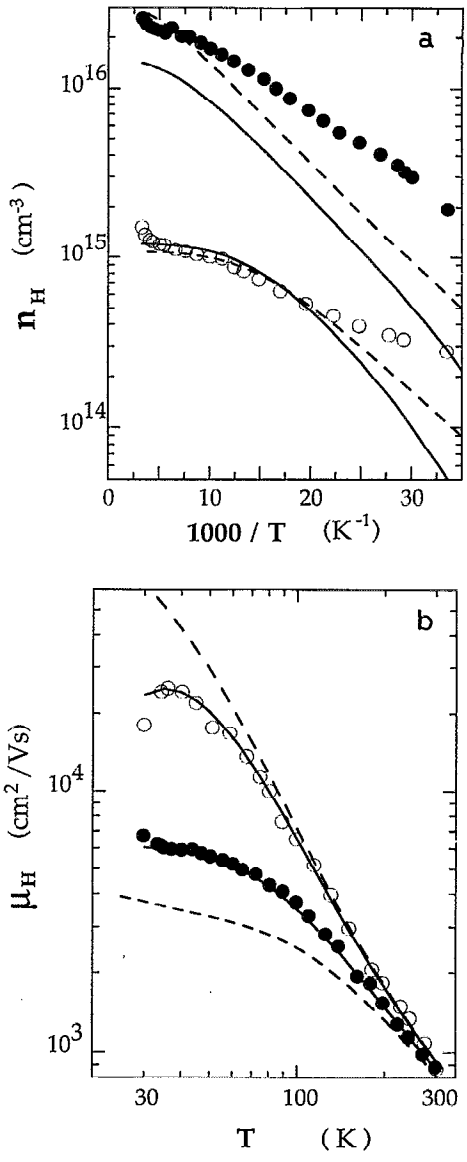

FIG. 4. Temperature dependence below RT of Hall (a) concentration and (b) mobility for an annealed 0.01% Sn-doped sample. Solid circles correspond to the observed dependence immediately after the annealing and the open circles to that measured after 1 week. Calculated curves assume either a single donor (dashed lines) or donor-acceptor (solid lines) model.

from 300 to 600 K and down to 300 K. It can be observed that the slope is higher when temperature decreases from 600 to 300 K, leading to an increase of the RT Hall mobility after the heating cycle. The temperature dependence of those magnitudes in the measurement cycle turns out to depend on the tin content, and then on the departure RT concentration.

In particular, we observe that the temperature at which the value of n_H (RT) begins to grow increases with increasing the tin content [Fig. 2(a)]. The highest tin content samples [$n_H(\mathrm{RT}) \gtrsim 10^{16}$ cm^{-3}] do not exhibit this effect. The Hall mobility curves of some samples from the 0.01% Sn-doped ingot [those with μ_H(RT) lower than 400 cm^2/V s] exhibit a maximum [open circles in Fig. 2(b)]. Some other samples from the 0.01% and 0.03% Sn-doped ingots [with μ_H(RT) between 400 and 500 cm^2/V s] present a mobility curve which tends to be constant above 400–500 K [open squares in Fig. 2(b)]. In the other samples (from 0.1%, 1%, 3%, and 10% Sn-doped ingots), the mobility curves exhibit a linear variation in the double logarithmic plot in all the temperature range, eventually with different slopes.

Figure 3 summarizes the $\mu_H(n_H)$ values at room temperature for all the samples. We can observe a great dispersion of the data points corresponding to the samples with lower tin content (0.01%–0.03%). The 0.1% Sn-doped samples are characterized by data points more concentrated at $n_H \approx 5\times10^{15}$ cm^{-3} and μ_H between 500 and 700 cm^2/V s. After a cycle of increasing-decreasing temperature the data points concentrate at about 2×10^{16} cm^{-3} with Hall mobility values of about 600 cm^2/V s. Annealed samples show the same values of n_H but higher mobilities (800–900 cm^2/V s).

Figure 4 shows the typical variation of n_H and μ_H between 30 and 300 K, on annealed 0.01% Sn-doped samples. The value of n_H(RT) relaxes from 10^{16} to nearly 10^{15} cm^{-3} (value before annealing) a week after annealing, as we can see from Fig. 4(a). On the contrary, the value of the Hall mobility at 300 K remains nearly constant after several days [$\approx$900 cm^2/V s in Fig. 4(b)]. The maximum of the μ_H curve takes place at lower temperature after relaxation [Fig. 4(b)] and its value grows from 6000 to about 20 000 cm^2/V s, also of the same order of magnitude than before annealing. It can be outlined that the annealing dynamics is several orders of magnitude faster than that of the relaxation: 10^3 s as compared to 10^6 s.

Resistivity curves along the c axis are plotted in Fig. 5 as a function of the temperature (300–700 K). We can observe a large decrease of this magnitude at RT with increasing Sn content, in agreement with previous results using these materials.[9] In each sample from the weaker Sn-doped ingots (0.01%, 0.03%, and 0.1%) we can ob-

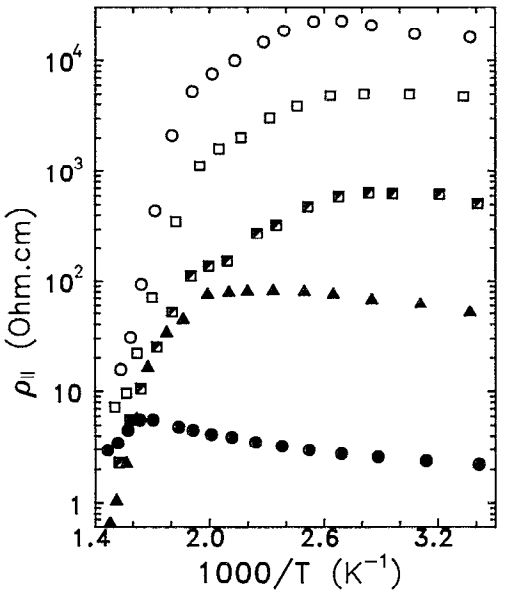

FIG. 5. Arrhenius plot of the resistivity parallel to the c axis in the high-temperature region for samples of the different Sn-doped ingots: (○) 0.01%, (□) 0.03%, (◪) 0.1%, (▲) 1%, and (○) 3%.

serve three well-differentiated zones: (i) 300–385 K, characterized by a weak variation with temperature; (ii) between 385 and 500 K we can observe a faster decrease, which can be compared with the increase observed in the same temperature range for the Hall concentration curves; (iii) above 500 K the resistivity exhibits an activated decrease with large activation energies ($\approx$1 eV), in contrast with the evolution of n_H which saturates above this temperature.

The higher-doped samples do not exhibit this behavior (although the 1% Sn-doped sample slightly does), and only a weak increase with increasing temperature is observed.

B. Far-infrared absorption

Figure 6(a) shows the absorption spectra for an undoped sample before and after annealing. Figure 6(b) shows the spectra before and after annealing for a 0.03% Sn-doped sample, and also the absorption spectrum of a 0.1% unannealed sample. The spectra of 0.01% Sn-doped samples are quite similar to those of the 0.03% samples and they are not shown. The main absorption lines in all spectra, correspond to the $1s$-$2p_{\pm}$ dipole transition.[3] Only one $1s$-$2p_{\pm}$ transition at an energy of about 102.5 cm^{-1} [Fig. 6(a)] is observed in undoped samples, associated with interstitial In atoms in the crystal.[1-3] This transition is also observed in the weakly Sn-doped samples, which also shows the $1s$-$2p_{\pm}$ transition associated with substitutional Sn atoms at about 113 cm^{-1} [Fig. 6(b)]. The integrated absorption of the main absorption lines in these samples increases up to an order of magnitude after annealing, as we can observe from the spectra shown in Figs. 6. An increase of the integrated absorption with increasing tin content is also observed as shown in Fig. 6(b). The absorption line at the lower-energy side of the main peaks in the spectra taken after annealing is related to donor pairing. The other one at 125 cm^{-1} (not resolved for the 0.03% sample) corresponds to the $1s$-$3p_{\pm}$ transition.

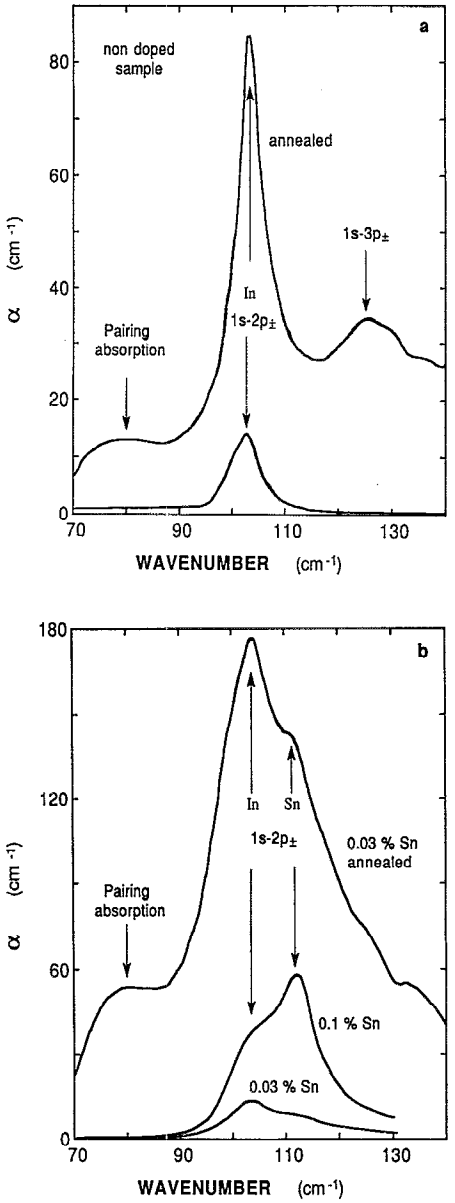

FIG. 6. Measured absorption due to optical transitions of electrons bound to shallow donor impurities in (a) undoped samples and (b) weakly Sn-doped samples, before and after annealing.

If we take the theoretical value of the oscillator strength corresponding to the $1s$-$2p_{\pm}$ (In and Sn) transition (0.31 and 0.29, respectively), we will be able to calculate the concentration of each donor type (In or Sn) from the integrated absorption intensity,[3] as follows.

(i) The native donor (interstitial indium) concentration is about 1.6×10^{14} cm^{-3} in the undoped and 0.03% Sn-doped samples before annealing, and 4×10^{14} cm^{-3} in the 0.1% Sn-doped sample. The Sn-related donor concentration grows almost an order of magnitude from the

0.03% (1.4×10^{14} cm^{-3}) to the 0.1% sample (9×10^{14} cm^{-3}).

(ii) After annealing, the In donor concentration is 9×10^{14} cm^{-3} in the undoped sample and 4×10^{15} cm^{-3} in the 0.03% Sn-doped sample. The Sn donor concentration in the last sample is now 2×10^{15} cm^{-3}.

IV. DISCUSSION

The existence of a naturally occurring 2D gas in InSe is well established. Areal electron concentrations of about 10^{11} cm^{-2} have been measured at low temperature in undoped samples,[4,10–12] and determine the measured Hall concentration below 20–30 K, which usually is found to be $\gtrsim10^{14}$ cm^{-3}.[1,13] Hence, the mean distance between the planar defects, where 2D electrons are confined, is estimated to be $d_m\leqslant10$ μm. At the same time we have inferred from far-infrared measurements that the shallow impurity concentration in either undoped or low-tin-content samples is about 10^{14} cm^{-3}. Why is Hall concentration at room temperature one order of magnitude higher than both 2D and 3D electron concentrations?

In Ref. 5 it was shown that the calculated RT 2D electron mobility is about one order of magnitude lower than the corresponding 3D one. Let us compare the data points of Fig. 3 with calculated curves in the 3D limit. Details of the calculation and scattering mechanisms involved have been extensively discussed in Ref. 5. Curve 1 represents the case without compensation and curve 2 the case of a compensation degree of 0.6, because it has been shown that tin atoms can also give place to acceptor impurities.[3,8,14] We observe that only the annealed and high-tin-content samples exhibit a 3D character, lower tin content (0.01 and 0.03%) being far away from this character and exhibiting 2D charge transport.[5] At the same time, when these low-tin-content samples are annealed for some minutes at about 300 °C, a great generation of shallow donors occurs, as deduced from Fig. 6. The origin of this shallow impurity generation and the 2D charge transport at RT can be thought to be the same: The existence of a large concentration of deep impurities probably adsorbed to the stacking faults, as was assumed in Refs. 5 and 15 to explain transport measurements. If we multiply the shallow impurity concentration after annealing ($\approx10^{16}$ cm^{-3}) by the mean distance between defects (1–10 μm) we can estimate such a deep impurity concentration to be about 10^{12}–10^{13} cm^{-2}, also in correspondence to the order of magnitude given in those works.[5,15] As these deep impurities are ionized electrons are excited to 2D subbands, which allows the growth of the 2D electron concentration from 10^{11} cm^{-2} at low temperatures to 10^{12} cm^{-2} at 300 K.[5]

The temperature dependence of μ_H and n_H below 300 K on annealed samples confirms their 3 D character in the charge transport. Mobilities are calculated by using the 3D model of Ref. 5. The following calculated curves have been superimposed.

(i) Curves with a continuous line are calculated by assuming a certain compensation degree for reproducing the experimental mobility curves. The mobility fitting parameters are: $N_D-N_A=1.5\times10^{16}$ cm^{-3}, $X_A=0.02$ for the sample measured after annealing and $N_D-N_A=1.22\times10^{15}$ cm^{-3}, $X_A=0.15$ when measured 1 week later. The 3D electron concentration has been calculated using the same parameters and assuming a single donor-acceptor model (the two shallow levels corresponding to In and Sn impurities have been reduced to only one with ionization energy $E_D\approx18.5$ meV):

$$n_{3D}(T)=\frac{1}{4}\left(\left\{\sqrt{\left[2N_A+N_C\exp\left(-\frac{E_D}{kT}\right)\right]^2+8N_C(N_D-N_A)\exp\left(-\frac{E_D}{kT}\right)}-\left[2N_A+N_C\exp\left(-\frac{E_D}{kT}\right)\right]\right\}^{1/2}\right). \quad (1)$$

(ii) Curves with dashed lines are calculated assuming a single donor model [Eq. (1) with $N_A=0$], with an energy of 18.5 meV for the shallow level. In this case we have used a donor concentration that reproduces the experimental electron concentration at room temperature: $N_D=2.5\times10^{16}$ cm^{-3} for the sample measured after annealing and $N_D=1.2\times10^{15}$ cm^{-3} when measured 1 week later.

If we compare the calculated curves with the experimental results in the case of the relaxed sample (after 1 week) we will find a satisfactory agreement above 50 either with or without compensation, which confirm that 3D electrons dominate in the sample for this temperature range. On the other hand, we must also pay attention to the strong disagreement below 50 K (the experimental curve tends to saturate), which only can be explained if 2D electrons ($\approx2\times10^{14}$ cm^{-3}) dominate for this other temperature range, and whose transport properties have been studied elsewhere.[15]

No agreement seems to exist between calculated and experimental Hall concentration curves in the case of the sample measured after annealing. This effect cannot be related to 2D electrons. Indeed, the 3D character in the sample measured immediately after annealing is more evident than after relaxation, because the experimental electron concentration does not tend to saturate below 50 K due to the higher difference between the shallow impurity concentration and the 2D electron concentration. The origin of this apparent disagreement can be found in the concentration curves: The experimental slope in the Arrhenius plot is lower than the calculated one. The most likely explanation for this effect is that interstitial In impurities can interact for such relatively high donor concentrations, which

consequently lowers their ionization energy. The increase of the overlap between electron wave functions of neighbor donors can be more effective for interstitial impurities given their greater capability of diffusion. In fact, this is suggested by the absorption spectra in the far-infrared region (Fig. 6): An absorption line is observed at 80 cm^{-1}, whose integrated intensity is about 25% of the main absorption line ($1s$-$2p_{\pm}$ transition), and attributed to impurity pairing.[3] At the same time this large absorption by impurity pairs make the impurity concentration deduced from the integrated intensity of the $1s$-$2p_{\pm}$ line to be underestimated by almost 50% (the oscillator strength of the $1s$-$2p_{\pm}$ transition must also be about 25% lower). Therefore, the real impurity concentration is in fact higher than that estimated in Sec. III B and closer to the concentration deduced from HE measurements.

Further information about the kinetics of impurities above room temperature, responsible for the observed annealing process, can be deduced from the results shown in Figs. 1 and 2. The most striking example of the effect of that kinetics corresponds to the Hall mobility curves of some 0.01% Sn-doped samples, like that shown in Fig. 2(b), which exhibits a maximum at about 400 K. At the same time this curve represents the clearest example of a change in the dimensionality of the charge transport. Let us assume the Hall mobility and concentration can be expressed with the approximation of zero magnetic field for two different kinds of carriers[5]

$$\mu_H=(n_2\mu_2^2+n_3\mu_3^2)/(n_2\mu_2+n_3\mu_3), \tag{2}$$

$$n_H=(n_2\mu_2+n_3\mu_3)^2/(n_2\mu_2^2+n_3\mu_3^2), \tag{3}$$

where the subscripts 2 and 3 refer to 2D and 3D electrons, respectively, $n_2=n_s/d_m$ being the effective volumic 2D electron concentration. Now the aforementioned curve can be explained if the ratio n_3/n_2 strongly increases with temperature, given that μ_2 and μ_3 decrease potentially. That is, 3D electrons become more and more important with increasing temperature and finally change the dimensionality of the charge transport from near 2D to 3D. The same conclusion is obtained from the curves of Fig. 1, in which a notable increase of the values of n_H and μ_H at RT is observed only by heating the sample up to 300 °C for a short time. Indeed, we also observe that by maintaining the sample at such a temperature for a time interval between 30 and 60 min, the Hall concentration remains nearly constant about 10^{16} cm^{-3} while the Hall mobility increases almost a 20%. This "3D enhancing" comes from the great generation of shallow donor impurities that takes place above room temperature, whose maximum effect is observed after an annealing process at about 300 °C for 30–60 min.

The temperature variation of the 2D and 3D electron concentrations above 300 K can be roughly estimated from the experimental curves of $n_H(T)$ and $\mu_H(T)$. However, several assumptions must be taken into account in order to avoid the great number of unknown microscopic parameters involved as follows:

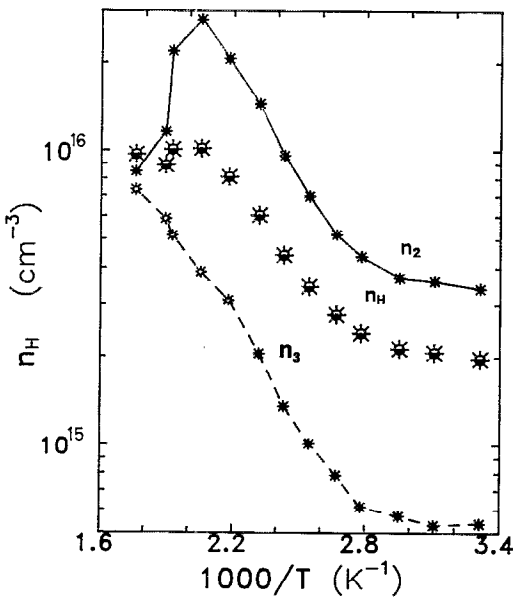

FIG. 7. Variation of the three- and two-dimensional electron concentrations above RT for an undoped sample, estimated from the directly accessible curves of n_H and μ_H.

(i) Only the first 2D subband is occupied. This assumption involves that only intraband scattering is present, which is less evident with increasing temperature. This approximation produces a subestimation of the 2D mobility.

(ii) The 2D electron concentration is of the order of 10^{12} cm^{-2} at room temperature. This value is explained by the ionization of the deep impurities in the planar defects and it is necessary in order to have a volumic 2D electron concentration larger than the shallow impurity concentration.[5]

(iii) Only phonon scattering mechanisms are considered to calculate the 2D and 3D mobilities. This approximation over-estimates the 2D mobility, given the high ionized impurity concentration in the planar defects.

The curves deduced in this way are shown in Fig. 7, corresponding to an undoped sample. The curve corresponding to 3D electrons corroborates the large increase of the shallow donor impurities with increasing temperature above 300 K. At the same time, an increase of the 2D electron concentration is also observed simultaneously, which can be lower if the 2D mobility is underestimated. The saturation in the $n_H(T)$ curve is related to the decrease of the 2D electron concentration, because the shallow impurity concentration is still increasing. On the other hand, the temperature dependence of n_3 is observed to be activated above 400 K. The observed activation energies are always of the order of 200 meV and are related to the escape energy of deep impurities out of the planar defects. The increase of the shallow impurity concentration with increasing tin content [Fig. 6(b)] makes the effect of the diffusion of deep impurities to be less important up to a higher temperature, if the thermal escape energy is similar in all ingots. As a consequence, an increase of the threshold temperature for the n_H curves with increasing tin content is

expected as was observed experimentally [Fig. 2(a)]. Simultaneously, a 3D enhancing of the charge transport should be verified, as is also observed in Fig. 2(b). The random nature of the stacking fault occurrence and the final concentration of deep impurities adsorbed to them explains the great dispersion observed in $\mu_H(n_H)$ data for low-tin-content samples, in which a 2D charge transport was dominant at RT.

The temperature dependence of the resistivity parallel to the c axis can be also understood within the picture of an impurity diffusion process from their initial sites at the stacking faults. The resistivity along the c axis comes from the motion of 3D electrons in this direction. In fact, if this concentration is about 10^{14} cm^{-3}, as we deduced before, the resistivity will be of the order of 100 Ω cm, up to two orders of magnitude lower than that observed for less Sn-doped samples between 300 and 400 K. Thus, it is obvious that we need to take into account the probability of electrons to tunnel through the potential barriers associated to the stacking faults, which prevent 3D electrons from moving along the c axis. Within this hypothesis, the resistivity could be expressed by

$$\rho_{\parallel}(T)=\frac{1}{en_3\mu_{3\parallel}}T_B(kT)^{-1}, \tag{4}$$

where $\mu_{3\parallel}$ is the 3D electron mobility parallel to the c axis, calculated like the perpendicular one but using $m_{\parallel}^{*}$, the electron effective mass parallel to the c axis, and $T_B(kT)$ the tunneling probability at the lattice temperature. This magnitude is then calculated by integrating the tunneling probability $T_B(E)$ with the Maxwell–Boltzmann distribution function. The calculation of $\rho_{\parallel}$ involves unknown microscopic parameters, such as the barrier heights and widths, and no calculations will be presented.

When deep impurities escape out of the planar defects and diffuse, resistivity is observed to decrease as shallow impurity concentration increases. This decrease is activated with activation energies comparable to those observed in the $n_H(T)$ curves up to 500 K. The resistivity in this temperature region can be explained by Eq. (4) with a constant value for $T_B(kT)$ of about 10^{-2}, which is reasonable for nonresonant tunneling across the planar defects. This is not the case when temperature increases above 500 K, because of the large activation energy observed in this high-temperature region ($\approx$1 eV). The large decrease of the resistivity can be related to a strong increase of the tunneling probability, given the slow growth of n_3 (Fig. 7) and the slow decrease of $\mu_{3\parallel}$ with increasing temperature. In our opinion, the phenomenology observed in the resistivity across the planar defects is analogous to the resonant tunneling transport problem in double-barrier heterostructures.[16]

V. CONCLUSIONS

In summary, we have carried out in this work a systematic study of the charge transport and shallow impurity distribution in InSe above room temperature or after an annealing process. We have corroborated the hypothesis used in previous works, related to the dimensionality of the electron transport and the existence of deep impurities, which are assumed to be adsorbed to stacking faults in this material. These impurities can diffuse above room temperature for occupying shallow donor positions in bulk InSe. The increase of 3D electrons by several orders of magnitude changes the dimensionality of the electron transport that was near 2D for undoped or weakly Sn-doped samples at room temperature, in which the initial concentration of shallow donors was as low as 10^{14} cm^{-3}. Resistivity measurements parallel to the c axis below 500 K are in agreement with the results along the perpendicular direction and have been qualitatively explained in terms of tunneling transport across the barriers associated to the stacking faults, which separates the electron depleted ϵ zones from the γ bulk.

ACKNOWLEDGMENTS

This work was supported through Spanish Government CICYT Grant No. MAT90-0242. J.M.P. wishes to thank Professor C. Sebenne and Professor M. Balkanski for their hospitality during his stay at the Laboratoire de Physique des Solides (Université Paris VI), where the far-infrared measurements were performed. Also, thanks are due to the facilities obtained from the group of Dr. C. Julien of this laboratory.

[1] A. Segura, K. Wünstel, and A. Chevy, Appl. Phys. A **31**, 139 (1983).
[2] R. M. De la Cruz, R. Pareja, A. Segura, and A. Chevy, J. Phys. C **21**, 4403 (1988).
[3] J. Martinez-Pastor, A. Segura, C. Julien, and A. Chevy, Phys. Rev. B **46**, 4607 (1992).
[4] J. C. Portal, R. J. Nicholas, E. Kress-Rogers, A. Chevy, J. M. Besson, J. Galibert, and D. Perrier, J. Phys. Soc. Jpn. Suppl. A **49**, 879 (1980).
[5] A. Segura, B. Marí, J. Martinez-Pastor, and A. Chevy, Phys. Rev. B **43**, 4953 (1991).
[6] A. Chevy, J. Cryst. Growth **67**, 119 (1984).
[7] A. Chevy, J. Appl. Phys. **56**, 978 (1984).
[8] B. Marí, A. Segura, and A. Chevy, Appl. Phys. A **45**, 579 (1988).
[9] F. Pomer, X. Bonet, A. Segura, and A. Chevy, Phys. Status Solidi B **145**, 261 (1988).
[10] G. L. Belenkii, M. O. Godzaev, and V. N. Zvereev, Pis'ma Zh. Eksp. Teor. Fiz. **43**, 594 (1986) [JETP Lett. **43**, 769 (1986)].
[11] N. B. Brandt, V. A. Kulbachinskii, Z. D. Kovalyuk, and G. V. Lashkarev, Fiz. Tekh. Poluprovodn. **21**, 1001 (1987) [Sov. Phys. Semicond. **21**, 613 (1987)].
[12] G. L. Belenkii, E. A. Vyrodov, and V. N. Avereev, Nuovo Cimento D **11**, 1571 (1989).
[13] A. Segura, F. Pomer, A. Cantarero, W. Krause, and A. Chevy, Phys. Rev. B **29**, 5708 (1984).
[14] B. Marí, A. Segura, and A. Chevy, Phys. Status Solidi B **130**, 793 (1985).
[15] J. Martinez-Pastor, A. Segura, and A. Cantarero, Solid State Commun. **81**, 287 (1992).
[16] Federico Capasso, Ed., *Physics of Quantum Electron Devices*, Springer Series in Electronics and Photonics, Vol. 28 (Springer, Berlin, 1990).